C. R. Mecanique 347 (2019) 912–919

Contents lists available at ScienceDirect

Comptes Rendus Mecanique

www.sciencedirect.com

Measurement of the relative air permeability of compacted earth in the hygroscopic regime of saturation

Antonin Fabbri *, Noha Al Haffar, Fionn McGregor

LTDS, UMR 5513 CNRS, ENTPE, 69518 Vaulx-en-Velin, France

ARTICLE INFO

Article history:
Received 28 June 2019
Accepted 13 November 2019
Available online 25 November 2019

Keywords:
Earthen materials
Relative permeability
Steady-state
Darcy's law
Vapor advection

ABSTRACT

The hygroscopic behavior of earthen materials has been extensively studied in the past decades. However, while the air flow within their porous network may significantly affect the kinetics of vapor transfer and thus their hygroscopic performances, few studies have focused on its assessment. For that purpose, a key parameter would be the gas permeability of the material, and its evolution with the relative humidity of the air. Indeed, due to the sorption properties of earthen material, an evolution of the water content, and thus of relative permeability, are foreseeable if the humidity of in-pore air changes. To fill this gap, this paper presents the measurement of relative permeabilities of a compacted earth sample with a new experimental set-up. The air flow through the sample is induced with an air generator at controlled flow rate, temperature, and humidity. The sample geometry was chosen in order to reduce, as much as possible, its heterogeneity in water content, and the tests were realized for several flow rates. The results, which show the evolution of gas permeability with the relative humidity of the injected air and with the water content of the material, either in adsorption or in desorption, were eventually successfully compared to predictions of the well-known Corey's law.

1. Introduction

In the general context of global warming, earthen constructions are regaining interest, mainly due to their attractiveness in terms of their low embodied energy [1,2] and for their high potential to contribute to a "passive" regulation of the interior climate of dwellings and other buildings [3–6]. Each construction can potentially be built with a different material and cannot be totally included in an industrial process. Therefore, several construction techniques have been invented, adapting them to the nature of the soil used. Among these techniques, the three most common ones are adobe blocks, cob and rammed earth [7]. But, whatever the construction technique, strong similarities exist in the soils used. For instance, all earthen materials used are described as a porous media with a relatively high permeability and with a solid matrix composed of non-negligible amount of clays, therefore allowing good vapor sorption properties [8]. The affinity of earthen materials to water also induces substantial complexity in their mechanical behavior. Indeed, in addition to the drop in strength commonly observed at high water content values [9], recent studies have underlined that significant changes in the mechanical behavior (strength variations, shrinkage, swelling) may be observed under normal operating conditions due

* Corresponding author.
E-mail address: antonin.fabbri@entpe.fr (A. Fabbri).

https://doi.org/10.1016/j.crme.2019.11.017

Table 1
Hygroscopic parameters of the samples.

Symbol	Description	Value [unity]
ϕ	Porosity	0.26
ρ_d	Dry density	1.97 [g/cm^3]
ρ_s	Specific density	2.7 [g/cm^3]
δ_p	Diffusion coefficient of vapor	4.2×10^{-11} [kg/m/Pa/s]

to the modification of the relative humidity of the air [10–12]. In consequence, a first step to correctly assess the behavior of earthen walls is the precise quantification of the humidity field within the in-pore air and within the material. [13].

For that purpose, the main equations that describe the hygroscopic couplings are nowadays quite well known by the scientific community (cf. [14,15], for example). But one of the main challenges remains the proper estimation of the material parameters that drive these mass transport equations, such as the vapor transfer coefficient [16], the isothermal sorption–desorption curve [17,18], as well as the liquid and gas relative permeabilities [19].

In particular, the increasing development of research activities on mass transfer through earthen materials has highlighted the strong lack in the literature of measurements of relative gas permeability in the hygroscopic range of saturation. This can be explained by the fact that advection of vapor due to gas transport is almost always neglected. But this quite common simplification has not got any consensus, since some authors have already underlined that air flows may have a significant impact on the hygroscopic behavior of porous material like concrete [20], textiles [21], or even earthen and bio-based materials [22].

In this context, this paper presents the development of an experimental set up to measure the relative permeabilities of a compacted earth sample. The air flow through the sample was induced with a humid air generator at controlled flow rate, temperature, and humidity. The testing protocol, including the definition of the sample geometry, is presented in the first part. Then, the results concerning gas permeability as a function of the relative humidity of the injected air and the water content, either in adsorption or in desorption, are presented and compared to predictions through the well-known Corey law [23].

2. Material characterization and preparation

2.1. Raw earth material and sample realization

The earthen material presented in this study is sampled from the rammed earth walls of an existing construction located in the South-East of France during operations of opening new doors and windows. This choice ensures that the studied material is suitable for building sustainable earth constructions. Particle size distribution, Atterberg limits, and methylene blue value were measured. The results show a mass content of clay (particles with a diameter lower than 2 μm) equal to 16%, a plasticity index of 14%, and a blue value of 2.7.

Cylindrical samples of 3.5 cm in diameter and 7 cm in height were manufactured at the optimum moisture content, resulting in maximum dry density (11% and 1.97 g/cm^3). Those parameters were previously determined using a manual CEB press. More details on the sample realization protocol are given in [10]. Just after their production, the samples were dried at 23 °C in a desiccator with silica gel until a constant mass was reached. The relative humidity within the desiccator was checked with a portable sensor (Rotronic HygroLog HL-NT), and it was found to be consistently lower than 5% RH.

2.2. Porous and hygroscopic properties

After the drying period, the cylinders were weighed and measured in order to estimate their dry density. Their specific density and their porosity were measured with a nitrogen pycnometer. The obtained values are reported in the Table 1.

Adsorption–desorption curves were measured using the Dynamic gravimetric Vapor Sorption method, commonly called the DVS method. It consists in measuring uptake and loss of moisture by flowing a carrier gas at a specified relative humidity (or partial pressure) over a small sample (from several milligrams to several grams, depending on the device used) suspended from the weighing mechanism of an ultrasensitive recording microbalance. Variations in the gas' relative humidity are automatically calculated by the device when the target condition in mass stability is reached. The results are reported in Fig. 1.

Water vapor permeability was measured using the wet cup method, following the procedure described in [16]. The vapor pressure gradient is created for the wet cup by setting the RH at 60% in the chamber and 85% in the cup. It leads to the values reported in Table 1.

Since this study focuses on the hygroscopic regime of saturation (saturation degree lower than 20%), the impact of liquid water transport was neglected and liquid permeability was not measured.

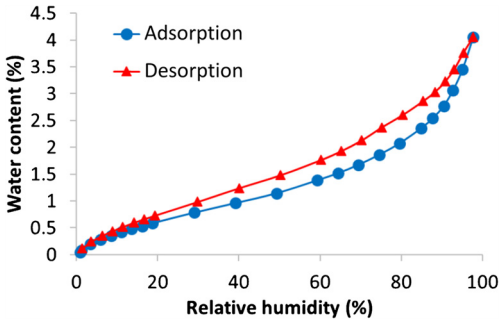

Fig. 1. Adsorption and desorption curves at 23 °C of the tested material obtained with the DVS method.

3. Experimental method to measure gas permeability

3.1. Intrinsic and relative permeability

Gas permeability, denoted by κ_G, characterizes the ability of a fluid mass to move through the porosity of a material. For an isotropic medium, and neglecting the influence of gravity, the mass flow of the gas can be written in the form:

$$\underline{\omega_G} = -\rho_G \frac{\kappa_G}{\eta_G} \underline{\nabla} P_G \tag{1}$$

where $\underline{\omega_G}$ is the mass flow vector, η_G is the viscosity of the gas, P_G its pressure and ρ_G its density, which is assumed to satisfy the perfect gas relation:

$$\rho_G = \frac{M_G}{RT} P_G \tag{2}$$

The value of gas permeability depends on the geometry of the porous network, which may change when the material deforms, and on the volumetric proportion of the pore space occupied by adsorbed and/or condensed water molecules [24]. The present study is limited to unloaded materials, which remain in the hygroscopic range of saturation. Thus the impact of the material deformation can reasonably be neglected and, for an isotropic medium, gas permeability can be written in the form:

$$\kappa_G = \kappa_G^0 \kappa_G^r(w) \tag{3}$$

where κ_G^0 is intrinsic permeability, that is, gas permeability for a totally dried sample, and $\kappa_G^r(w)$ is relative permeability, which is a function of the water content, denoted by w. For the record, the water content is defined as the mass of water divided by the dry mass of the solid.

3.2. Set up of the experimental device

Several methods exist to estimate intrinsic permeability, mainly transient methods [25] or steady-state methods [26]. Indirect estimation methods, based on the upscaling of transfers within the interconnected pores at several levels, have also been developed [27].

In this paper, a steady-state approach is chosen. When low saturation ratios are considered, the main difficulty of this method is to be able to generate flows of gas and/or liquid while keeping a constant and homogeneous saturation state through the sample. To overcome this problem, one method, already used to assess the liquid relative permeability of cement-based materials [28] and the relative gas permeability of textiles [29], consists in fixing the water content of the material through the relative humidity of the incoming air. Indeed, as it is depicted by the sorption curves (cf. Fig. 1), any increase of the relative humidity of the air will increase its water content.

For that purpose, an experimental device quite similar to the one developed by Gibson et al. [29] for textile applications was set up. It is made of a static triaxial cell (GDS/CEL/STA/100) with drainage systems on its cap and base pedestal. They are linked to a wet-air generator (WETSYS S60/59105) at constant flow rate, varying between 5 mL/min and 200 mL/min, depending on relative humidity, which varies between 0% and 95%, at a temperature between ambient and 50 °C. A special climatic chamber was built to contain the cell and regulate its temperature (accuracy of 0.1 °C). The wet air can be injected in the sample through its bottom side or its top side, while the other side is kept at atmospheric pressure. The inlet/outlet pressures, temperatures and relative humidity are monitored during the whole test. A diagram of the experimental device is reported in Fig. 2.

Using this device, the gas at controlled relative humidity was injected at constant flow rate within the material. The difference between the inlet and outlet pressures, respectively denoted by $P_{G,i}$ and $P_{G,o}$, was recorded. When this latter

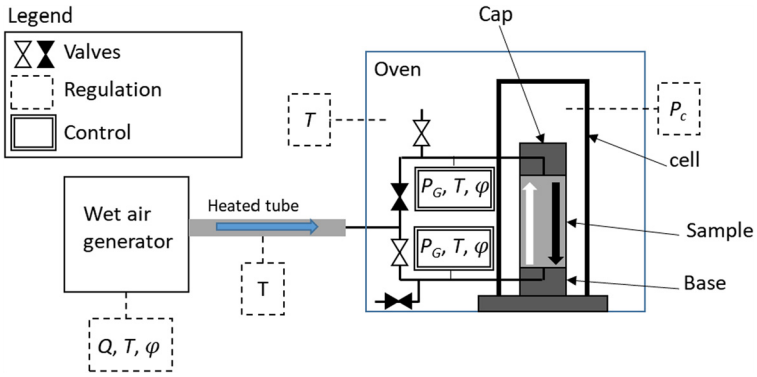

Fig. 2. Schematic diagram of the experimental device. The black arrow through the sample represents the direction of the gas flow when the black valves are open and the white valves are closed, and reciprocally for the white arrow. P_c is the confinement pressure in the cell, T the temperature, Q the volumetric flow rate, φ the relative humidity, and P_G the gas pressure.

became constant, the steady state was assumed to be reached. To ensure an unidirectional flow and to avoid leakage at the interfaces with the base and the cap, the sample was jacketed in an impermeable latex membrane, and a confinement pressure of 1 bar is applied, which remains at least twice the inlet overpressure. Given the bulk modulus of the materials, which is higher than 300 MPa even for a relative humidity of 97% [11], the volumetric strain induced by the confinement pressure is of the order of 10^{-4}; therefore, the impact on the transport properties is assumed to be negligible.

3.3. Principle of measurement, sample geometry and maximum flow rate

Under steady-state conditions, if the water content is homogeneous through the sample, the mass conservation of the gas phase (that is $\underline{\nabla} \cdot \underline{\omega_G} = 0$), combined with (1–2) leads to:

$$\kappa_G = \kappa_0 \kappa_G^r(w) = Q\ \eta_G\ \frac{2HP_{G,i}}{A(P_{G,i}^2 - P_{G,o}^2)} \tag{4}$$

where H is the sample's thickness, A its cross surface, and Q is the incoming volumetric gas flow rate ($Q = \rho_{G,i}\,\underline{\omega_G} \cdot \underline{n}$, with $\rho_{G,i}$ the density of the incoming gas and $\underline{n}$ the outgoing normal vector).

On the other side, if the water content is not homogeneous through the sample, the mass conservation of the air does not directly provide permeability, but its average value. In consequence, a good control of the heterogeneity in water content, and thus of the relative humidity of the air, through the sample is necessary for an accurate measurement of gas permeability. For that purpose, the flow of vapor mass within the sample, which is denoted by $\underline{\omega_V}$, must be assessed precisely. Considering both vapor advection and diffusion processes, $\underline{\omega_V}$ satisfies:

$$\underline{\omega_V} = \frac{\rho_V}{\rho_G}\underline{\omega_G} - P_G \delta_p \underline{\nabla}\left(\frac{\varphi p_V^s}{P_G}\right) \tag{5}$$

where φ is the relative humidity of the in-pore air, p_V^s the pressure of the vapor at saturation and ρ_V its apparent density, which is assumed to satisfy the perfect gas relation:

$$\rho_V = \frac{M_w}{RT}\varphi p_V^s \tag{6}$$

In (5), the term $(\rho_V/\rho_G)\underline{\omega_G}$ represents the mass of vapor advected by the gas phase, while $-P_G\delta_p\underline{\nabla}(p_V/P_G)$ is the diffusion of vapor within the gas phase. If the incoming flow of air is in the order of 10 mL/min, the order of magnitude of the mass of vapor advected by the gas phase within the sample of cross section $A = 10$ cm^2 is 10^{-5} kg/s/m^2. On the other side, considering the material parameters of Table 1, the diffusive flow for a variation of relative humidity of 0.1 within a 1-cm-thick sample is in the order of 10^{-6} kg/s/m^2. At first order, the latter can thus be neglected.

Under this assumption, the combined use of relations (1–6), the mass conservation equations ($\underline{\nabla} \cdot \underline{\omega_G} = 0$ and $\underline{\nabla} \cdot \underline{\omega_V} = 0$), and relation (4) allows us to express the relative difference between outlet and inlet relative humidity at constant temperature, denoted by r_φ, in the form:

$$r_\varphi = \frac{\varphi_o - \varphi_i}{\varphi_i} = \frac{1}{\chi}\left(\sqrt{1+\chi^2}+1\right) - 1 \tag{7}$$

where φ_o and φ_i are respectively the outlet and the inlet relative humidity while χ is a dimensionless number, which is a function of the permeability of the material, of its geometry (thickness and cross section), of the flow rate and of the outlet pore pressure.

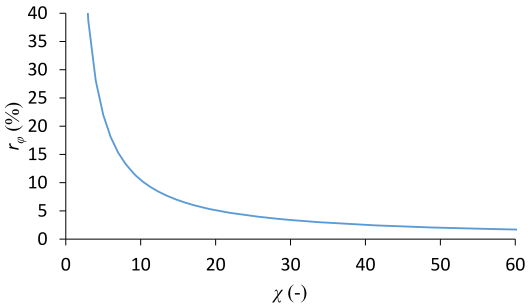

Fig. 3. Evolution of r_φ with χ.

It is equal to:

$$\chi = \frac{\kappa_0 < \kappa_G^r >}{\eta_G} \frac{A P_{G,o}}{Q H} \tag{8}$$

The evolution of r_φ with χ is reported in Fig. 3. To insure a good homogeneity in water content through the sample, r_φ must be as low as possible, and thus χ must be as high as possible.

Since the outlet pressure and the sample surface are fixed, the only parameters on which it is possible to act to increase χ are gas flow and sample thickness, which should be both as small as possible. The lower flow rate that can be reached while keeping a good regulation with our system is 10 mL/min. On the other side, in order to avoid a too important inlet overpressure, Q will be limited to 25 mL/min.

Under these conditions, and assuming permeability values higher than 1×10^{-14} m^2, a sample thickness of 1 cm would lead to values of χ higher than 12.7 and r_φ lower than 8%. This relative variation, which is in the range of uncertainty of the relative humidity sensors, is considered as acceptable.

3.4. Test protocol

The first stage consists in applying through the sample a flow of dry air at 25 mL/min. When the permanent state is reached (stable relative humidity and pressure at inlet and outlet), the flow is progressively reduced to 10 mL/min by steps of 5 mL/min. For each step, the inlet and outlet pressures were recorded and the permeability coefficient was estimated using Eq. (4) as long as the permanent state was reached. Even if permeability measurements were made at different flows, the outlet overpressure remained equal to 0, while the inlet overpressure was limited to 0.5 bar. Due to these technical constrains, the mean pressure variations remained quite limited, and it was not possible to study Klinkenberg's effect [30]. In consequence, only the apparent gas permeability was measured in this study.

4. Results of gas permeability measurements

Gas permeabilities measured for all testing configurations are summarized in Table 2. At first, the tests performed at the several flow rates underline its limited impact in the range of values considered in this study (which are between 10 and 25 mL/min). This result gives some confidence in the accuracy of the measurements, particularly with regard to those of the inlet and outlet pressures.

Whatever the relative humidity of the injected air, permeabilities in the range of 10 mD (10^{-14} m^2) were observed. This emphasizes the permeable nature of the tested material. Indeed, it is in the gas permeability range of permeable rocks like Vosges sandstones [31], while being at least three orders of magnitude higher than that of cement-based materials [32].

This result is interesting by itself. Indeed, given this high gas permeability value, the mass transfer of vapor through the material by an air advection process might not be negligible if gas pressure variations, caused by wind effect for example, are considered. Anyway, it underlines that this point deserves to be analyzed.

Nonetheless, even if they remained in the same order of magnitude, a noticeable reduction of gas permeability was observed when the relative humidity of the injected air increases. For the record, injection of dry air led to permeability values 35% higher than those observed with injection of wet air at 90% HR. This variation may not be negligible if in-pore vapor advection needs to be considered to have a correct estimation of the humidity field within the material, especially since it is in the range of relative humidity that may be observed during the lifetime of an earthen wall.

To analyze further these results, the average relative humidity, defined as the arithmetic mean between the inlet and outlet relative humidities, was rather considered. It is supposed to be representative of the average humidity within the sample. Due to the quite limited gradient of relative humidity within the sample, this approach, though simplified, is considered sufficient.

The variation of gas permeability with the average relative humidity is reported in Fig. 4A. Interestingly, a difference is observed between permeability values that were measured during the adsorption and desorption stages. Because gas

Table 2
Summary of the results obtained for the several relative humidity and air flow. φ_{in} is the relative humidity of the injected air, φ_{moy} is the average between the inlet and outlet relative humidity while $\Delta\varphi$ denotes the difference between the inlet and outlet relative humidity.

φ_i [%]	Q [mL/min]	φ_{moy} [%]	$\Delta\varphi$ [%]	κ_G [mD]
Adsorption stage				
0.5	24.88	1.1	1.3	11.74
0.5	19.97	1.2	1.4	11.76
0.8	14.64	1.4	1.2	11.6
1.8	9.80	2.3	0.4	12.1
29.1	24.67	26.7	4.8	10.68
29.2	19.75	26.8	4.8	10.61
30.0	14.76	27.2	5.6	10.64
29.5	9.78	27.2	4.7	10.77
57.0	24.67	52.0	10.0	9.94
56.8	19.46	52.0	9.6	9.83
56.7	14.67	51.9	9.6	9.80
56.4	9.66	51.6	9.6	9.90
90.9	24.62	81.5	18.8	8.61
88.9	19.46	80.6	16.7	8.49
91.4	14.67	81.7	19.3	8.42
91.3	9.66	81.5	19.7	8.49
Desorption stage				
57.3	24.67	52.8	9.0	9.41
57.8	19.75	53.0	9.6	9.37
58.5	14.71	53.3	10.5	9.29
57.4	9.69	52.4	9.9	9.38
29.6	24.96	27.3	4.7	10.24
29.2	19.61	27.2	4.1	10.03
29.2	14.67	27.2	4.1	10.01
29.2	9.71	27.2	4.0	10.50
0.3	24.85	1.1	1.5	11.02
0.7	19.84	2.0	2.5	10.91
1.2	14.92	2.3	2.1	10.93
1.9	9.91	2.7	1.7	11.12

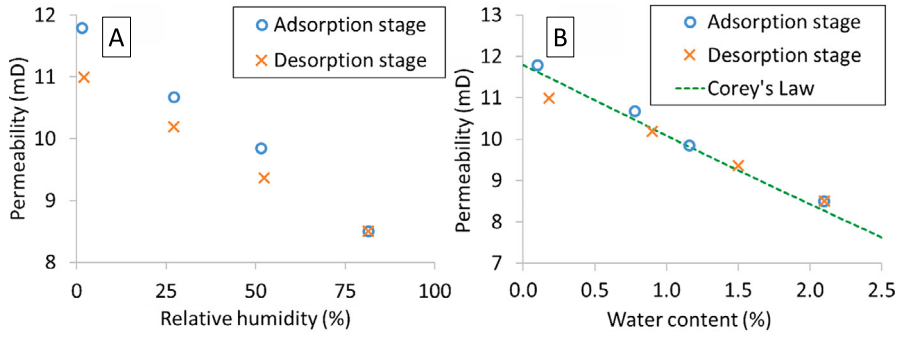

Fig. 4. Evolution of gas permeability with relative humidity (A) and water content (B). Permeability is expressed in mD ($1\ \text{mD} \approx 1.0 \cdot 10^{-15}\ \text{m}^2$).

permeability should rather be driven by the water content than by the relative humidity of the air (cf. Eq. (3)), this may be a consequence of the hysteresis between adsorption and desorption curves, as it is depicted in Fig. 1. This assumption seems verified by the results presented in Fig. 4B, in which almost no more difference was observed between the adsorption and desorption stages if gas permeability is expressed as a function of the water content instead of the relative humidity. For this graph, the water content was not directly measured, but it was calculated from the average relative humidity, using either the adsorption or the desorption curves, depending on the stage that is considered.

5. Discussion on the evolution of relative air permeability with liquid saturation

The variation of gas permeability with water saturation can be attributed to several phenomena. A first one, which was already observed in textile materials by [33], can be the modification of the microstructure due to swelling processes.

However, this explanation might not be consistent with the quite limited volumetric swelling, lower than 0.005%/%rh, which was measured in [34] for similar compacted earth samples (same earth, similar dry density, same compaction procedure).

A second explanation can rise up from the analysis of the porous network structure of the material. As it was discussed in [19], it should be composed by large pores connected to each others by narrow throats. Adsorption of water molecules at the pore walls when the relative humidity of the air increases may thus fill some of these narrow throats. As a consequence, the number of percolation pathways through the material for the gas phase would be reduced, which translates, at the macroscopic scale, by a reduction of gas permeability. To go further on that point, it could be interesting to analyze more in detail the shape of the relation between gas permeability and liquid ratio. For that purpose, several theoretical and empirical laws have been already developed [25]. Among them, one of the most used is Corey's law [23], which can be written in the form:

$$\kappa_G = \kappa_G^0 (1 - S_r)^2 (1 - S_r^2) \tag{9}$$

where S_r is the reduced saturation ratio, which can take into account the impact of both liquid and gas residual saturations. If these two terms are considered to be null, and if the deformation of the material is neglected, S_r can be linked to the water content, denoted by w, through the relation:

$$S_r = w \frac{\rho_d \rho_s}{\rho_s - \rho_d} \tag{10}$$

The comparison between the predictions obtained with relations (9–10) and the experimental results is reported in Fig. 4B. A good consistency is observed, even though no calibration parameters were used, since both residual liquid and gas saturations were assumed to be null.

Even if it is not a formal proof, the fact that Corey's law was initially established from experimental data for non-swelling porous materials and for oil and gas in-pore phases (instead water and air) tends to give some confidence in the assumption that the variation of permeability is rather induced by the filling of some narrow pores with liquid water than by swelling phenomena.

Finally, to interpret properly this result, it is important to underline that, for a given hydric state, the water content value depends on the method that is used to reach the reference dry state of the sample (that is, for which $w = 0$). For example, it was shown in [17] that earthen samples will have a lower mass after being dried in an oven at 105 °C than after being dried by a flow of dry air at 23 °C. In this study, a flow of dry air at 23 °C was used to determine the dry mass of the samples. As a consequence, to obtain the same results while considering a dry mass from oven-drying at 105 °C, it would be necessary to take into account a non-null residual saturation in the expression of S_r. In view of the definition of a standardized method to estimate a consistent dry mass of earthen materials, these results, although they need to be further investigated, may be quite interesting.

6. Conclusion

In this paper, a novel apparatus to measure the evolution of the gas permeability of earthen material in the hygroscopic range of saturation was presented. From the analysis of the water vapor transport within the porous network of the material, limits on sample thickness and flow rate of the injected wet air were determined. The obtained results were analyzed in terms of water content and relative humidity. Corey's law was found to fit accurately the experimental results, without the needs of any calibration parameters. As a consequence, at least for the same kind of sample than the one studied here (compacted fine earth with no gravels, quite high dry density), a single measurement of intrinsic gas permeability can be sufficient to estimate the variation of gas permeability with water content in the hygroscopic range of saturation.

References

[1] J. Morel, A. Mesbah, M. Oggero, P. Walker, Building houses with local materials: means to drastically reduce the environmental impact of construction, Build. Environ. 36 (2011) 1119–1126.
[2] A. Arrigoni, C. Beckett, D. Ciancio, G. Dotelli, Life cycle analysis of environmental impact vs. durability of stabilised rammed earth, Constr. Build. Mater. 142 (2017) 128–136.
[3] M. Hall, D. Allinson, Analysis of the hygrothermal functional properties of stabilised rammed earth materials, Build. Environ. 44 (2009) 1935–1942.
[4] M. Woloszyn, T. Kalamees, M. Abadie, M. Steeman, A.S. Kalagasidis, The effect of combining a relative-humidity-sensituve ventilation system with the moisture buffering capacity of materials on indoor climate and energy efficiency of buildings, Build. Environ. 44 (2009) 515–524.
[5] M. Labat, C. Magniont, N. Oudhof, J. Aubert, From the experimental characterisation of the hygrothermal properties of straw-clay mixtures to the numerical assessment of its buffering potential, Build. Environ. 97 (2016) 69–81.
[6] T. Busser, M. Pailha, A. Piot, M. Woloszyn, Simultaneous hygrothermal performance assessment of an air volume and surrounding highly hygroscopic walls, Build. Environ. 148 (2019) 677–688.
[7] M. Hall, R. Lindsay, M. Krayenhoff, Modern Earth Buildings, Woodhead, 2012.
[8] F. McGregor, A. Heath, A. Shea, The moisture buffering capacity of unfiered clay masonry, Build. Environ. 82 (2014) 599–607.
[9] Q.B. Bui, J.C. Morel, S. Hans, P. Walker, Effect of moisture content on the mechanical characteristics of rammed earth, Constr. Build. Mater. 54 (2014) 163–169.
[10] F. Champiré, A. Fabbri, J. Morel, H. Wong, F. McGregor, Impact of hygrometry on mechanical behavior of compacted earth for building constructions, Constr. Build. Mater. 110 (2016) 70–78.

[11] L. Xu, K. Wong, A. Fabbri, F. Champiré, D. Branque, Loading-unloading shear behavior of rammed earth upon varying clay content and relative humidity conditions, Soil Found. 58 (2018) 1001–1015.
[12] A. Bruno, C. Perlot, J. Mendes, D. Gallipoli, A microstructural insight into the hygro-mechanical behaviour of a stabilised hypercompacted earth, Mater. Struct. 51 (2018) 32.
[13] A. Fabbri, J. Morel, D. Gallipoli, Assessing the performance of earth building materials: a review of recent developments, RILEM Tech. Lett. 3 (2018) 46–58.
[14] M. Labat, M. Woloszyn, Moisture balance assessment at room scale for four cases based on numerical simulations of heat–air–moisture transfers for a realistic occupancy scenario, J. Build. Performance Simulation 9 (2016) 487–509.
[15] L. Soudani, A. Fabbri, J. Morel, M. Woloszyn, P. Chabriac, H. Wong, A. Grillet, A coupled hygrothermal model for earthen materials, Energy Build. 116 (2016) 498–511.
[16] F. McGregor, A. Fabbri, J. Ferreira, T. Simoes, P. Faria, J.C. Morel, Procedure to determine the impact of the surface film resistance on the hygric properties of composite clay/fibre plasters, Mater. Struct. 50 (2017).
[17] A. Fabbri, F. McGregor, I. Costa, P. Faria, Effect of temperature on the sorption curves of earthen materials, Mater. Struct. 50 (2017) 253.
[18] R. Bui, M. Labat, J. Aubert, Comparison of the saturated salt solution and the dynamic vapor sorption techniques based on the measured sorption isotherm of straw, Constr. Build. Mater. 141 (2017) 140–151.
[19] A. Fabbri, L. Soudani, F. McGregor, J. Morel, Analysis of the water absorption test to assess the intrinsic permeability of earthen materials, Constr. Build. Mater. 199 (2019) 154–162.
[20] V. Baroghel-Bouny, M. Mainguy, T. Lassabatere, O. Coussy, Characterization and identification of equilibrium and transfer moisture properties for ordinary and high-performance cementitious materials, Cem. Concr. Res. 29 (1999) 1225–1238.
[21] P. Gibson, A. Elsaiid, C.K.D. Rivin, M. Charmchi, A test method to determine the relative humidity dependence of the air permeability of textile materials, J. Test. Eval. (1997).
[22] J. Berger, S. Gasparin, D. Dutykh, N. Mendes, On the solution of coupled heat and moisture transport in porous material, Transp. Porous Media 121 (2018) 665–702.
[23] A. Corey, The interrelation between gas and oil relative permeability, Prod. Mon. 19 (1954) 38–41.
[24] M. Monfared, J. Sulem, P. Delage, M. Mohajerani, Temperature and damage impact on the permeability of opalinus clay, Rock Mech. Rock Eng. 47 (2014) 101–110.
[25] E. Dana, F. Skoczylas, Gas and stones permeability and pore structure of sandstones, Int. J. Rock Mech. Min. Sci. 36 (1999) 613–625.
[26] F. Osselin, A. Fabbri, T. Fen-Chong, J. Pereira, A. Lassin, P. Dangla, Experimental investigation of the influence of supercritical state on the relative permeability of vosges sandstone, C. R., Méc. 343 (2015) 495–502.
[27] J. Carmeliet, F. Descamps, G. Houvenaghel, A mutliscale network model for simulating moisture transfer properties of porous media, Transp. Porous Media 35 (1999) 67–88.
[28] S. Zamani, R. Kowalczyk, P. McDonald, The relative humidity dependence of the permeability of cement paste measured using nmr profiling, Cem. Concr. Res. 57 (2014) 88–94.
[29] P. Gibson, M. Charmchi, Modeling convection/diffusion processes in porous textiles with inclusion of humidity-dependent air permeability, Int. Commun. Heat Mass Transf. 24 (1997) 709–724.
[30] J. Klinkenberg, The permeability of porous media to liquids and gases, in: Drilling and Production Practice, 1941.
[31] F. Osselin, T. Fen-Chong, A. Fabbri, A. Lassin, J. Pereira, P. Dangla, Dependence on injection temperature and on aquifer's petrophysical properties of the local stress applying on the pore wall of a crystallized pore in the context of co_2 storage in deep saline aquifers, Eur. Phys. J. Appl. Phys. 64 (2013) 21101.
[32] A. Fabbri, J. Corvisier, A. Schubnel, F. Brunet, B. Goffé, G. Rimmele, V. Barlet-Gouédard, Effect of carbonation on the hydro-mechanical properties of portland cements, Cem. Concr. Res. 39 (2009) 1156–1163.
[33] P. Gibson, D. Rivin, C. Kendrick, H. Schreuder-Gibson, Humidity-dependent air permeability of textile materials, Tex. Res. J. 69 (1999) 311–317.
[34] A. Fabbri, F. Champiré, L. Soudani, F. McGregor, H. Wong, Poromechanics of compacted earth for building applications, in: Poromechanics 2017 - Proceedings of the 6th Biot Conference on Poromechanics, 2017.